

Tuning the type of charge carriers in N-heterocyclic carbene-based molecular junctions through electrodes

Ming-Lang Wang(王明郎), Chuan-Kui Wang(王传奎)

Citation: Chin. Phys. B . 2020, 29(11): 113101 . **doi:** 10.1088/1674-1056/aba277
Journal homepage: http://cpb.iphy.ac.cn; http://iopscience.iop.org/cpb

What follows is a list of articles you may be interested in

Phase separation and super diffusion of binary mixtures of active and passive particles

Yan Wang(王艳), Zhuanglin Shen(谌庄琳), Yiqi Xia(夏益祺), Guoqiang Feng(冯国强), Wende Tian(田文得)
Chin. Phys. B . 2020, 29(5): 053103 . **doi:** 10.1088/1674-1056/ab81f4

Control water molecules across carbon-based nanochannels

Xianwen Meng(孟现文), Jiping Huang(黄吉平)
Chin. Phys. B . 2018, 27(1): 013101 . **doi:** 10.1088/1674-1056/27/1/013101

Anisotropic self-diffusion of fluorinated poly(methacrylate) in metal-organic frameworks assessed with molecular dynamics simulation

Tao Lu(鲁桃), Biao Xu(徐彪), Fei-Hong Ye(叶飞宏), Xin-Hui Zhou(周馨慧), Yun-Qing Lu(陆云清), Jin Wang(王瑾)
Chin. Phys. B . 2017, 26(12): 123104 . **doi:** 10.1088/1674-1056/26/12/123104

Improvement of the thermoelectric efficiency of pyrene-based molecular junction with doping engineering

Mohammad Farid Jamali, Meysam Bagheri Tagani, Hamid Rahimpour Soleimani
Chin. Phys. B . 2017, 26(12): 123101 . **doi:** 10.1088/1674-1056/26/12/123101

Electronic transport properties of lead nanowires

Lishu Zhang(张力舒), Yi Zhou(周毅), Xinyue Dai(代新月), Zhenyang Zhao(赵珍阳), Hui Li(李辉)
Chin. Phys. B . 2017, 26(7): 073102 . **doi:** 10.1088/1674-1056/26/7/073102

Tuning the type of charge carriers in N-heterocyclic carbene-based molecular junctions through electrodes*

Ming-Lang Wang(王明郎)† and Chuan-Kui Wang(王传奎)

School of Physics and Electronics, Shandong Normal University, Jinan 250358, *China*

(Received 25 May 2020; revised manuscript received 21 June 2020; accepted manuscript online 3 July 2020)

Designing tunable molecular devices with different charge carriers in single-molecule junctions is crucial to the next-generation electronic technology. Recently, it has been demonstrated that the type of charge carriers depends on and can be tuned by controlling the molecular length and the number of interfacial covalent bonds. In this study, we show that the type of charge carriers can also be tuned by controlling the material and shape of electrodes. N-heterocyclic carbenes (NHCs) have attracted attention because of their ability to form strong, substitutional inert bonds in a variety of metals. Also, NHCs are more stable than the widely used thiol group. Therefore, we use electrodes to tune the type of charge carriers in a series of NHCs with different side groups. The *ab initio* calculations based on non-equilibrium Green's formalism combined with density functional theory show that the dominant charge carrier switches from electrons to holes when gold electrodes are changed into platinum ones. The nature of the charge carriers can be identified by variations in the transport spectra at the Fermi level (E_F), which are caused by the side groups. The projections of transport spectra onto the central molecules further validate our inferences. In addition, the transmission coefficient at E_F is found to be dependent on the atomic interface structure. In particular, for the NHC without methyl or ethyl side groups, connecting a protruding atom on the electrode surface significantly enhances the transportability of both electrode materials. Overall, this study presents an effective approach to modifying transport properties, which has potential applications in designing functional molecular devices based on NHCs.

Keywords: molecular electronics, charge carriers, side groups, non-equilibrium Green's function

PACS: 31.15.at, 73.63.–b **DOI:** 10.1088/1674-1056/aba277

1. Introduction

Over the past few years, single molecular electronics has aroused unprecedented interest as a promising alternative to conventional Si-based electronics.[1] Thus far, several remarkable functional single-molecule devices mimicking the functionality of typical electronic components have been theoretically designed and experimentally fabricated, such as single-molecule switches,[2–9] molecular diodes,[10–12] and field-effect transistors.[13–15] Complementary metal–oxide–semiconductor (CMOS) transistors consisting of p-type and n-type transistors are the fundamental building blocks of the modern semiconductor industry. To realize functional circuits like CMOS, it is vital to create and control both types of charge carriers. The type of molecular junction is defined according to the main charge carrier present: an electron for n-type and a hole for p-type. In an n-type (p-type) molecular junction, the unoccupied (occupied) molecular orbitals dominate the transmission. Charge carriers are generally dominated by the relative alignment of the frontier molecular orbitals and the Fermi level (E_F) of the electrodes in the molecular junctions.[16] Recently, Dell *et al.* tuned these types of charge carriers into a family of electron-deficient thiophene-1,1-dioxide (TDO) oligomers by controlling the number of TDO units.[17] Further, Low *et al.* fixed the length of TDO oligomers and altered the strength of electron acceptors in the molecular backbone to systematically switch their polarity,[18] whereas Jiang *et al.* utilized the variation in the number of C–C covalent bonds formed at graphene–porphine–graphene (GPG) molecular junctions to tune the polarity of charge carriers.[19] Additionally, varying the anchor groups between molecules and electrodes is an efficient strategy to realize different types of charge carriers. Notably, for Au electrodes, molecules terminated with pyridine group conduct through the lowest unoccupied molecular orbital (LUMO), while those terminated with thiolate group conduct through the highest occupied molecular orbital (HOMO).[20] Here, we demonstrate that controlling the material and shape of electrodes is another effective strategy to tune the polarity of charge carriers.

Since the initial report by Arduengo *et al.*,[21] N-heterocyclic carbenes (NHCs) have become one of the most investigated families of ligands because they can form strong, substitutional inert bonds in a variety of metals.[22–25] Compared with the widely utilized thiol group, which tends to degrade in air, light, or organic solvents,[26,27] NHCs can retain their stability within a wide pH range, in harsh conditions such as high temperature, and oxidizing environments.[28,29] Functionalized NHC–metal complexes play a vital role in cataly-

*Project supported by the National Natural Science Foundation of China (Grants Nos. 11874242 and 21933002) and the Shandong Provincial Natural Science Foundation, China (Grant No. ZR2019PA022).

†Corresponding author. E-mail: wangminglang@sdnu.edu.cn

© 2020 Chinese Physical Society and IOP Publishing Ltd

sis, surface protection, drug protection and delivery, sensing, surface-enhanced Raman spectroscopy, and electronics.[30–35] The binding mode of NHCs on metal surfaces can be tuned by the side groups. In the case of short alkyl side groups, the standing-up configuration is selected, whereas in the case of longer alkyl groups, the flat-lying configuration is the preferred orientation.[36] Although the bonding of NHCs to a metal surface via a protruding (adatom) site or an atop site provides much lower adsorption energy when the NHCs are perpendicular to the metal surface than when they are parallel,[37,38] the strong metal-C bond formed at the contact interface provides enhanced electronic coupling, which can facilitate the transfer of electrons from the electrodes to the molecules and *vice versa*. Compared with the thiol-modified metal surface, the NHC-modified metal surface is a very promising candidate in electronics due to its lower work function.[39] Recently, theoretical and experimental investigations have revealed that the conductance of NHC molecular junctions can be influenced by the shape of the tip and the linked metal atoms.[40,41] Further, to fully understand the transport properties of NHCs, it is necessary to investigate the effect of the electrodes.

In this work, we investigate the transport properties of NHC molecules with H, methyl, and ethyl side groups. The molecules are separately connected to the atop positions and adatom positions on Au (111) and Pt (111) surfaces. The side groups are used to change the energy levels of NHC molecules. This provides an excellent way to align the energy levels between the electrodes and molecules, similar to the way a gate electrode is used in molecular junctions. Changing the side groups from H to methyl to ethyl raises the energy levels of NHC molecules accordingly. In addition, we consider how these energy levels can be tuned by the nature of the electrodes. When the electrode is made of gold, the reduction in the transmission coefficient at E_F is ascribed to the LUMO of the isolated molecule. However, in the case of a platinum electrode, the increase in the transmission coefficient at E_F is attributed to HOMO-2. We design n-type and p-type molecular junctions by using NHC molecules through changing the electrodes from gold to platinum, which may be the basic building blocks for assembling future molecular circuits. We believe that our findings have potential applications in designing and tuning the type of charge carrier in molecular devices.

2. Theoretical model and methods

The supercell, describing the metal–molecule–metal junction, contains three parts: the left electrode, the right electrode, and the central scattering region, which are illustrated in Fig. 1. The Au (111) slabs containing three atomic layers on the left- and right-hand side are used to model the semi-infinite electrodes. A 4×4 periodicity is used in the *xy* plane with 16 atoms per layer. Except for the repetitive electrode region, the central scattering part contains NHC molecules with three different side groups: H(NHC–H), methyl(NHC–Me), and ethyl(NHC–Et) groups, whose structural formulas are shown in Fig. 1(a). They are symmetrically connected to the atop positions and adatom positions on the Au surface through flanked carbon atoms, which are shown in Fig. 1(b). Here, we refer to the atop position as the position in which the molecule connects directly to one atom on the metal surface, while we refer to the adatom position as the position in which the molecule connects to an atom protruding from the metal surface. In addition to the Au (111) electrode model, a similar model based on Pt (111) electrodes is also considered. All the structures of the devices discussed in this study except the Au-NHC(H)-Au molecular junctions are shown in Fig. S1.

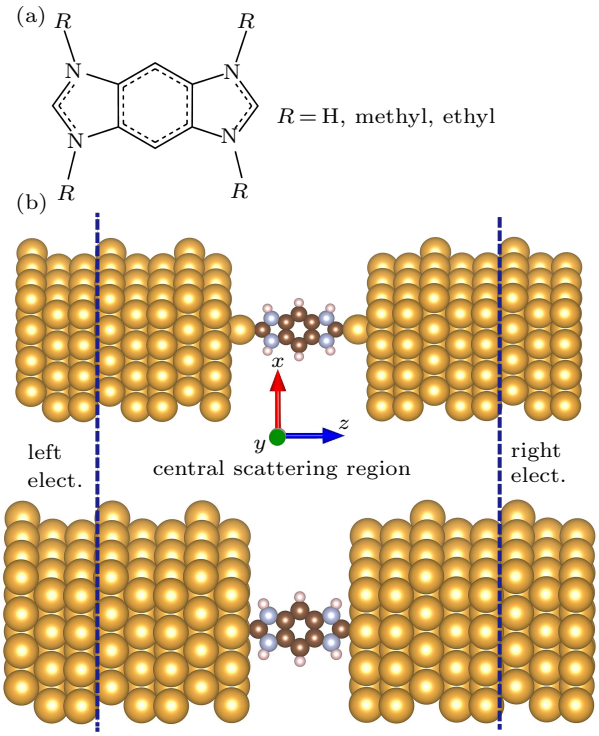


Fig. 1. (a) Molecular structure of NHC with substitutional side group *R*, which includes H, methyl, and ethyl groups. (b) Schematic diagram of molecular transport junction, with central molecular backbone being NHC molecule that is attached to atop position (down panel) and adatom position (up panel) on Au (111) surface.

Firstly, the NHC molecules whose side groups are changed from hydrogen into methyl to ethyl are optimized in the SIESTA package through the standard conjugation gradient method until the atomic forces are less than 0.03 eV/Å.[42–45] After constructing the metal–molecule–metal sandwich junctions, the same force criterion is adopted to relax these molecular junctions, where only the molecular bridge and two adjacent Au layers on the left- and right-hand sides are optimized. The following finite-range numerical basis sets are employed to describe the valence electrons: a double-zeta plus polarization (DZP) basis set for C, H, and N atoms, a DZP basis set extended with diffuse functions for Au

atoms on the surface, and a single-zeta plus polarization (SZP) basis set for bulk Au atoms. In the case of a Pt electrode, an SZP basis set is sufficient.[46] The exchange–correlation functional is based on the generalized gradient approximation (GGA) proposed by Perdew–Burke–Ernzerhof (PBE).[47,48] A density mesh cut-off of 200.0 Ry (1 Ry = 13.6056923(12) eV) is used for the real-space grid.

The transport properties are investigated by using a combination of non-equilibrium Green's function (NEGF) combined with density functional theory (DFT) approaches, which is implemented in the SMEAGOL package.[49–54] The elemental parameters are the same as those in the case of the relaxing process. To calculate the Green's function, 24 energy points along the semi-circle and 24 points along the line in the complex plane are employed. We use 24 poles for the Fermi function with an electronic temperature of 25 meV. The transmission spectrum $T(E)$ of the metal–molecule–metal junction is calculated from the following equation:

$$T(E) = \frac{1}{S_{2\mathrm{DBZ}}} \int_{2\mathrm{DBZ}} T(\boldsymbol{k};E)\,\mathrm{d}\boldsymbol{k}, \tag{1}$$

where $S_{2\mathrm{DBZ}}$ is the area of a two-dimensional Brillouin zone in the lateral direction, which is orthogonal to the transport direction. The transmission coefficient $T(\boldsymbol{k};E)$ is defined as follows:

$$T(\boldsymbol{k};E) = \mathrm{Tr}[\Gamma_{\mathrm{L}} G_{\mathrm{M}}^{\mathrm{R}} \Gamma_{\mathrm{R}} G_{\mathrm{M}}^{\mathrm{R}+}], \tag{2}$$

where $G_{\mathrm{M}}^{\mathrm{R}}$ is the retarded Green's function matrix of the central molecule, and Γ_{L} (Γ_{R}) is the broadening function or matrix that describes the interfacial interaction; subscript L (R) denotes the left-hand (right-hand) side interfaces. The k-point sampling with 4×4 k-points (one k-point) is employed in the periodic (transport) direction.

3. Results and discussion

We initiate the study by exploring the geometric and electronic structure of NHC molecules. The investigation of different side groups indicates that the atomic structure of the NHC backbone is almost the same for all the three molecules, where the length of the C–N bond is 1.37 Å, and that of the C–C bond in central benzene is 1.40 Å. However, as shown in Fig. 2, when the side group is changed from H to methyl to ethyl, the energy levels are gradually upshifted. The considerable rise in the energy levels from NHC–H to NHC–Me and a small increase from NHC–Me to NHC–Et can be understood based on the nature and intensity of electron-donation by the methyl and ethyl groups. The energy gap between the HOMO and LUMO is almost the same (∼ 3.15 eV) for NHC–H and NHC–Me, while for NHC–Et the energy gap is slightly smaller (∼ 3.07 eV). The frontier molecular orbitals of NHC–H are illustrated on the right panel in Fig. 2. The HOMO-2, LUMO, and LUMO+1 exhibit very delocalized electron distributions, each of which consists of p-orbitals from the N and C atoms of the NHC backbone. In contrast, in the case of HOMO and HOMO-1, the σ bond in the central phenyl component reduces the coupling between the lone pair orbitals of terminal C atoms. In particular, HOMO and HOMO-1 represent the same state distributions except the sign of the p-orbital of the terminal C atom, which is opposite on the right-hand side. A comparison of the states among NHC–H, NHC–Me, and NHC–Et is illustrated in Fig. S2, which reveals that these states are independent of the side groups. The effect of the side groups on the NHC backbone is similar to that of a gate electrode, which adjusts the movement of molecular energy levels. This provides a powerful way to identify the type of charge carriers in NHC-based molecular junctions.

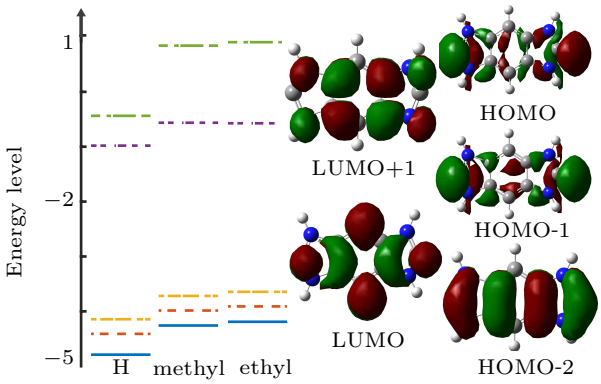


Fig. 2. Frontier molecular orbitals of isolated NHC molecule with side group H (right), and variation in energy levels when side group is changed from H to methyl and ethyl (left).

The equilibrium transmission spectra of NHC with three side groups located on the top of Au (111) surface are shown in Fig. 3(a). Overall, these spectra exhibit similar trends, *i.e.*, each of them has two prominent peaks and a long plain region (∼ 2.5 eV) crossing E_{F}. However, the transmission spectra shift toward higher energy positions as the side group changes from H to methyl to ethyl, which is consistent with the trend of molecular energy levels. At E_{F}, the transmission coefficient is $1.2\times10^{-2}\ G_0$ ($G_0 = 2e^2/h$, e is the electron charge and h is the Planck's constant) for NHC–H, $7.5\times10^{-3}\ G_0$ for NHC–Me, and $7.3\times10^{-3}\ G_0$ for NHC–Et, separately. This decreasing trend suggests that electrons may be the primary charge carriers, producing an n-type molecular junction. In the case of NHC–H, a narrow peak is located at −2.66 eV below E_{F}, and a broad peak is located at 0.90 eV above E_{F}. However, in the case of NHC–Me, the transmission peak below E_{F} is a superposition of a sharp peak and a broad peak. The sharp peak is observed to be at −2.21 eV, and the resonance peak is located at 1.23 eV above E_{F}. When the central molecule changes to NHC–Et, two peaks near E_{F} are observed to be at −2.21 eV and 1.27 eV, respectively. Considering the fact that the peak below E_{F} is far from E_{F} and decays sharply, it may be inferred that the resonance peak above E_{F} primarily contributes to the

transmission coefficient at E_F. It is the contribution coming from the unoccupied state that suggests that these molecular junctions are of n-type.

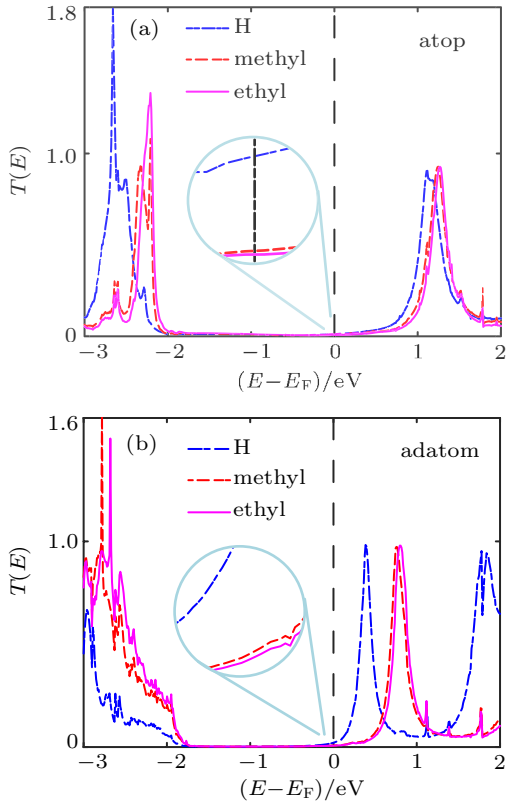


Fig. 3. Equilibrium transmission spectra at different contact positions on Au electrode surface: (a) atop position, (b) adatom position, with insets showing amplified transmission coefficient at E_F, and blue, red, and pink curves indicating H, methyl, and ethyl side groups at *R* position of NHC molecule, respectively.

When the adsorption position of Au is changed from an atop position to an adatom site, the overall trend of the transmission spectra is not reversed as shown in Fig. 3(b). However, the coupling strength becomes slightly weaker when the number of connecting Au atoms decreases from three to one. The energy corresponding to these peaks above E_F rises from 0.39 eV to 0.76 eV to 0.81 eV as the side group changes from H to methyl to ethyl, and the transmission coefficient at E_F decreases from 2.2×10^{-2} G_0 to 7.3×10^{-3} G_0 to 6.8×10^{-3} G_0, respectively. In the case of NHC–H, the change from an atop position to an adatom position shifts the peak above E_F to a position near E_F, which facilitates a significant enhancement in transmission coefficient at E_F in Au adatom. By contrast, in the case of NHC–Me and NHC–Et, the transmission coefficient at E_F decreases with respect to that at the Au atop position. The opposite trend has been reported earlier and can be rationalized in terms of the effect of interfacial structures.[55]

To obtain an insight into the nature of transport, we project the equilibrium transmission spectra onto the frontier molecular orbitals, to analyze the influence of interfacial structures and side groups on the transferring channel at E_F. For the case of Au at an atop position, the projections of NHC with different side groups are shown in Fig. 4. Remarkably, HOMO and HOMO-1 equally contribute to the transmission spectra, which can be understood by the same electron distributions shown in Fig. 2. The transmission spectra contributed by HOMO and HOMO-1 exhibit a plain region because the interfacial coupling is extremely strong. The peak located at −2.66 eV facilitates a conductance value of 1.8 G_0. It is dominated by HOMO-2 and HOMO-3 that provide two transport channels. The resonance peak above E_F, which contributes to a conductance of 1 G_0, is ascribed to the LUMO. Although the transmission coefficient at E_F contributed by HOMO and HOMO-1 are very similar to that by NHC–H and NHC–Me, the contribution of LUMO results in a smaller conductance value of 0.001 G_0 at E_F. Interestingly, the peak at HOMO-2 in NHC–Me is observed to be at a lower energy than that at HOMO-3. This indicates that the coupling between HOMO-2

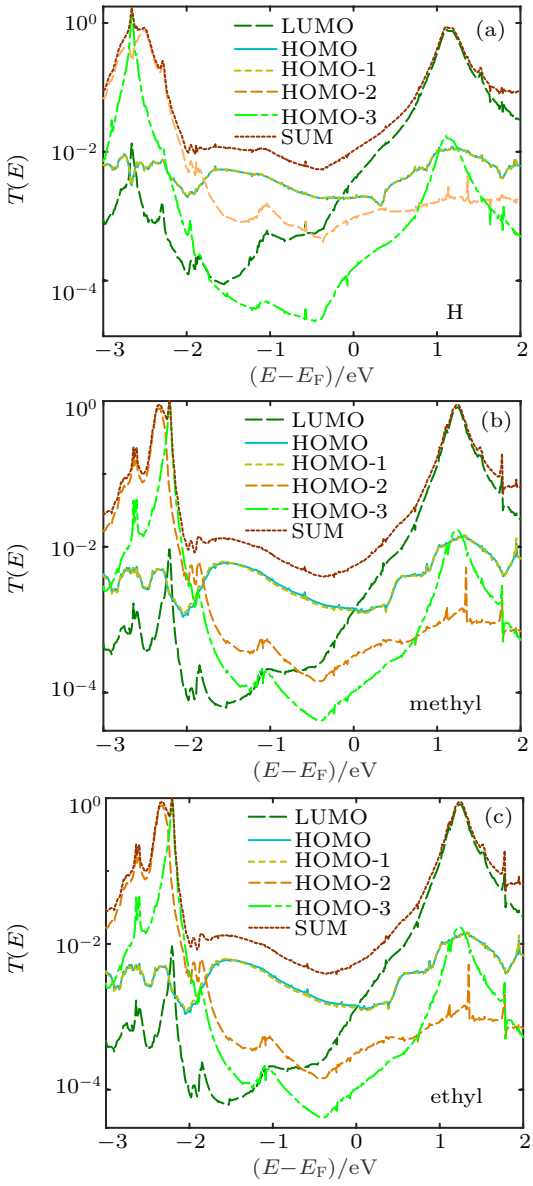


Fig. 4. Transmission spectra projected onto frontier molecular orbitals of NHC molecule, which are located at atop position on Au electrode surface with (a) H, (b) methyl, and (c) ethyl side groups.

and the energy states of the electrodes is strong, which causes the electrons transferring to the electrodes to be enhanced. For NHC–Et, the LUMO peak rises further, generating the smallest transmission coefficient at E_F. These observations are in agreement with the results obtained according to the projections in Fig. 3(a), which shows that the properties of the NHC molecules with methyl and ethyl side groups are similar. Even though the adsorption site of Au is changed from an atop position to an adatom position, the primary characteristics remain identical. Figure S3 shows that LUMO, which is closer to E_F, facilitates a higher conductance value. However, for NHC–Me and NHC–Et, the interfacial effect can counteract the effect of downward LUMO, resulting in a smaller transmission coefficient at E_F.

Recently, Zeng *et al*. successfully deposited an NHC molecule onto a Pt (111) surface to exhibit an extremely stable interfacial contact.[56] Due to the similar influences of methyl side group and ethyl side group on the transport properties, we investigate only Pt–NHC(H/Et)–Pt molecular junctions. When the NHC is located at a Pt-atop site, the length of the Pt–C bond is nearly 1.97 Å for NHC–H and 2.01 Å for NHC–Et. In Fig. 5(a), the Pt-(NHC–H)–Pt molecular junction exhibits three prominent peaks at 2.10 eV, −1.42 eV, and −1.72 eV, respectively. A broad distribution is observed between −0.88 eV and −2 eV, which indicates a high transmission coefficient. A flat curve above −0.88 eV, which is ∼ 2.25 eV long, exhibits an extremely small transmission coefficient. Considering the energy gap between the peaks near E_F and E_F, the conductance value of 7.7×10^{-3} G_0 at E_F can be attributed to the peaks below E_F. When the side group changes into ethyl, the peak below E_F shifts toward a higher energy, while the peak above E_F shifts toward a lower energy. Accordingly, the transmission coefficient at E_F increases to 9.3×10^{-3} G_0, which further validates our suggestion that these occupied orbitals contribute to the transmission. Figure 5(b) shows that in the case of the Pt adatom, the transmission coefficient contributed by the prominent peak above E_F is nearly the same (∼ 1.0 G_0), which is independent of the side groups. In contrast, the NHC–Et exhibits a higher conductance value under E_F. At E_F, the values of conductance for NHC–Et and NHC–H are 1.95×10^{-3} G_0 and 1.59×10^{-3} G_0, respectively. These results suggest that the upward peaks under E_F dominate the transmission coefficient at E_F. The weaker coupling that exists between molecular unoccupied orbitals and the Pt d-orbitals also appears between the three connecting metal atoms and the terminal C atom in the NHC molecule; this coupling strength becomes weaker when the number of connecting atoms decreases from three to one. The peaks under the Fermi level increase closer to the Fermi level because the higher Pt d-orbitals interact with the NHC molecule than the Au d-orbitals. In particular, when the NHC molecule is attached to the adatom position, the interaction between the molecular orbitals and the Pt d-orbitals is enhanced and results in a large increase in transmission coefficient at the Fermi level.

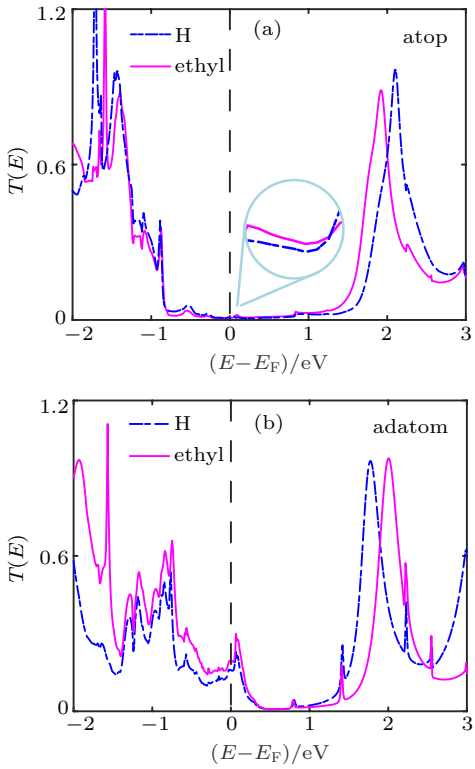


Fig. 5. Equilibrium transmission spectra at different contact positions on Pt electrode surface: (a) atop position and (b) adatom position. Inset in panel (a) shows amplified transmission coefficient at E_F. Blue and pink curves refer to H and ethyl side groups at the *R* position of the NHC molecule, respectively.

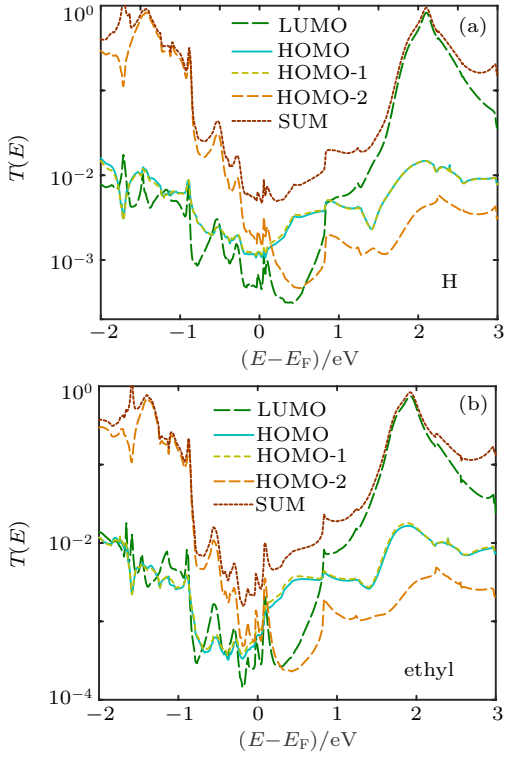


Fig. 6. Transmission spectra projected onto frontier molecular orbitals of NHC molecule, which is located at atop position on Pt electrode surface with (a) H and (b) ethyl (b) side groups.

Finally, we focus on the projections of the transport spectra onto the frontier molecular orbitals of NHC–H and NHC–Et to obtain a better understanding of the transport properties. These spectra (in logarithmic scale) are shown in Fig. 6 and Fig. S4. In the case of the Pt atop position, the transmission coefficients contributed by HOMO and HOMO-1 are equivalent to each other, which may be attributed to the electronic distribution of the frontier molecular orbitals. This scenario is similar to the one explained above. It is also clear that the peak above E_F is dominated by LUMO, while the transmission peaks under and at E_F are dominated by HOMO-2 of isolated NHC molecules (Figs. 2 and 6). In the case of NHC–Et, the higher conductance value at E_F is ascribed to the upward HOMO-2. Overall, we can conclude that the conductive holes are the dominant charge carriers at E_F. Figure S4 shows that when the interfacial structure changes to a Pt adatom position, the upward shifted HOMO-2 facilitates a higher conductance value at E_F. Therefore, when NHC–H and NHC–Et are connected to the Pt electrode, holes are the primary charge carriers, which suggests that the molecular junction is of p-type.

4. Conclusions

We employ a combination of DFT and NEGF to investigate the transport properties of the NHC molecule with three side groups (H, methyl, and ethyl groups) located at atop postions and adatom positions on Au (111) and Pt (111) surfaces. We observed that side groups can be used to adjust the energy levels of the NHC molecular backbone as well as the energy alignment between the electrodes and molecules. The properties can be further tuned by controlling the shape and material of the electrodes. When the side group changes from H to methyl to ethyl, the energy levels of the NHC molecule are upshifted accordingly. Notably, the transmission channel at E_F changes from HOMO-2 to LUMO for isolated molecules when the electrode material changes from gold to platinum. Consequently, we are able to design an n-type and a p-type molecular junction based on NHC molecules by changing the nature of the electrodes. We believe that our theoretical results provide an effective approach to tuning the type of charge carriers in molecular devices and to designing the next-generation functional molecular devices such as switches and memories.

References

[1] Xiang D, Wang X, Jia C, Lee T and Guo X 2016 *Chem. Rev.* **116** 4318

[2] Jia C, Migliore A, Xin N, Huang S, Wang J, Yang Q, Wang S, Chen H, Wang D, Feng B, Liu Z, Zhang G, Qu D, Tian H, Ratner M A, Xu H, Nitzan A and Guo X 2016 *Science* **352** 1443

[3] Mu Y, Zhao J, Chen L, Huang H, Wang M, Hu G, Wang C and Zhang G 2020 *Org. Electron.* **81** 105665

[4] Zuo M, Liao W H, Wu D and Lin L E 2019 *Acta Phys. Sin.* **68** 237302 (in Chinese)

[5] Yan R, Wu Z W, Xie W Z, Li D and Wang Y 2018 *Acta Phys. Sin.* **67** 097301 (in Chinese)

[6] Sun F, Liu R, Suo, Y Q, Niu L L, Fu H Y, Ji W F and Li Z L 2019 *Acta Phys. Sin.* **68** 178502 (in Chinese)

[7] Yi X H, Liu R, Bi J J, Jiao Y, Wang C K and Li Z L 2016 *Chin. Phys. B* **25** 128503

[8] He Z L, Bai J Y, Ye S J, Li L and Li C X 2018 *Chin. Phys. Lett.* **34** 087301

[9] Li Y Q, Kan, H J, Miao Y Y, Lei Y, Qiu S, Zhang G P, Ren J F, Wang C K and Hu G C 2020 *Chin. Phys. B* **29** 017303

[10] Zhang N, Lo W, Cai Z, Li L and Yu L 2017 *Nano Lett.* **17** 308

[11] Lopes C S, Merces L, de Oliverira R F, de Camargo D H S and Bufon C C B 2020 *Nanoscale* **12** 10001

[12] Capozzi B, Xia J, Adak O, Dell E Liu J Z, Taylor J C, Neaton J B, Campos L M and Venkataraman L 2015 *Nat. Nanotech.* **10** 22

[13] Song H, Kim Y, Jang Y H, Jeong H, Reed M A and Lee T 2009 *Nature* **462** 1039

[14] Xiang D, Jeong H, Kim D, Lee T, Cheng Y, Wang Q and Mayer D 2013 *Nano Lett.* **13** 2809

[15] Sun H, Liu X, Su Y, Deng B, Peng H, Decurtins S, Sanvito S, Liu S, Hou S and Liao J 2019 *Nanoscale* **11** 13117

[16] Zhan X, Facchetti A, Barlow S, Marks T J, Ratner M A, Wasielewski M R and Marder S R 2011 *Adv. Mater.* **23** 268

[17] Dell E J, Capozzi B, Xia J, Venkataraman L and Campos L M 2015 *Nat. Chem.* **7** 209

[18] Low J Z, Capozzi B, Cui J, Wei S, Venkataraman L and Campos L M 2017 *Chem. Sci.* **8** 3254

[19] Jiang Z, Wang H, Wang Y, Sanvito S and Hou S 2017 *J. Phys. Chem. C* **121** 27344

[20] Su T A, Neupane M, Steigerwald M L, Venkataraman L and Nuckolls C 2016 *Nat. Rev. Mater.* **1** 16002

[21] Arduengo III A J, Harlow R L and Kline M 1991 *J. Am. Chem. Soc.* **113** 361

[22] Sprick R S, Hoyos M, Morrison J J, Grace I M, Lambert C, Navarro O and Turner M L 2013 *J. Mater. Chem. C* **1** 3327

[23] An Y, Yu J and Han Y 2019 *Chin. J. Chem.* **37** 76

[24] Smith C A, Narouz M R, Lummis P A, Singh I, Nazemi A, Li C and Crudden C M 2019 *Chem. Rev.* **119** 4986

[25] Thanneeru S, Ayers K M, Anuganti M, Zhang L, Kumar C V, Ung G and He J 2020 *J. Mater. Chem. C* **8** 2280

[26] Yang G, Amro N A, Starkewolfe Z B and Liu G Y 2004 *Langmuir* **20** 3995

[27] Srisombat L, Jamison A C and Lee T R 2011 *Colloids Surf. A* **390** 1

[28] Vericat C, Vela M E, Benitez G, Carro P and Salvarezza R C 2010 *Chem. Rev.* **39** 1805

[29] Médard G and Papageorgiou A C 2019 *Nat. Chem.* **11** 17

[30] Zhukhovitskiy A V, Macleod M J, Johnson J A 2015 *Chem. Rev.* **115** 11503

[31] Han G, Ghosh P, Rotello V M 2007 *Nanomedicine* **2** 113

[32] Lv A, Freitag M, Chepiga K M, Schäfer A H, Glorius F and Chi L 2018 *Angew. Chem. Int. Ed.* **57** 4792

[33] Baquero E A, Tricard S, Coppel Y 2018 *Dalton Trans.* **47** 4093

[34] Ernst J B, Muratsugu S, Wang F, Rakers L, Lecante P, Philippot K, Chaudret B and Glorius F 2018 *Chem. Commun.* **54** 7070

[35] Dejesus J F, Trujillo M J, Camden J P and Jenkins D M 2018 *J. Am. Chem. Soc.* **140** 1247

[36] Bakker A, Timmer A, Kolodzeiski E, Freitag M, Gao H Y, Mönig H, Amirjalayer S, Glorius F and Fuchs H 2018 *J. Am. Chem. Soc.* **140** 11889

[37] Larrea C R, Baddeley C J, Narouz M R, Mosey N J, Horton J H and Crudden C M 2017 *ChemPhysChem* **18** 3536

[38] Rodriguez-Castillo M, Lugo-Preciado G, Laurencin D, Tielens F, van der Lee A, Clement S, Guari Y, Lopez-de-Luzuriaga J M, Monge M, Remacle F and Richeter S 2016 *Chem. Eur. J.* **22** 10446

[39] Kim H K, Kyla A S, Winget P, Li H, Wyss C M, Jordan A J, Larrain F A, Sadighi J P, Fuentes-Hernandez C, Kippelen B, Brédas J, Barlow S and Marder S R 2017 *Chem. Mater.* **29** 3403

[40] Foti G and Vázquez H 2016 *Nanotechnology* **27** 125702

[41] Doud E A, Inkpen M S, Lovat G, Montes E, Paley D W, Steigerwald M L, Vázquez H, Venkataraman L and Roy X 2018 *J. Am. Chem. Soc.* **140** 8944
[42] Meir Y and Wingreen N S 1992 *Phys. Rev. Lett.* **68** 2512
[43] Hohenberg P and Kohn W 1964 *Phys. Rev.* **136** B864
[44] Xue Y, Datta S and Ratner M A 2002 *Chem. Phys.* **281** 151
[45] Brandbyge M, Mozos J, Ordejón P, Taylor J and Stokbro K 2002 *Phys. Rev. B* **65** 165401
[46] Soler J M, Artacho E, Gale J D, García A, Junquera J, Ordejón P and Sánchez-Portal D 2002 *J. Phys.: Condens Matter* **14** 2745
[47] Perdew J. P, Burke K and Ernzerhof M 1996 *Phys. Rev. Lett.* **77** 3865
[48] Zhang G, Xie Z, Song Y, Wei M, Hu G and Wang C 2017 *Org. Electron.* **48** 29
[49] Rocha A R, García-Suárez V M, Bailey S W, Lambert C J, Ferrer J and Sanvito S 2005 *Nat. Mater.* **4** 335
[50] Miao Y, Qiu S, Zhang G, Ren J, Wang C and Hu G 2018 *Phys. Rev. B* **98** 235415
[51] Wei M Z, Wang Z Q, Fu X X, Hu G C, Li Z L, Wang C K and Zhang G P 2018 *Physica E* **103** 397
[52] Zhang G P, Mu Y Q, Zhao J M, Huang H, Hu G C, Li Z L and Wang C K 2019 *Physica E* **109** 1
[53] Li Z L, Bi J J, Liu R, Yi X H, Fu H Y, Sun F, Wei M Z and Wang C K 2017 *Chin. Phys. B* **26** 098508
[54] Liu R, Bi J, Xie Z, Yin K, Wang D, Zhang G, Xiang D, Wang C and Li Z 2018 *Phys. Rev. Appl.* **9** 054023
[55] Foti G and Vázquez H 2016 *Nanotechol.* **27** 125702
[56] Zeng Y, Zhang T, Narouz M R, Crudden C M and McBreen P H 2018 *Chem. Commun.* **54** 12527